BIOLOGICAL CRYSTALLOGRAPHY

ISSN 1399-0047

Structure of the bovine COPI δ subunit μ homology domain at 2.15 Å resolution

Avital Lahav,[a] Haim Rozenberg,[b] Anna Parnis,[c] Dan Cassel[c]* and Noam Adir[a]*

[a]Schulich Faculty of Chemistry, Technion, Haifa 32000, Israel, [b]Department of Structural Biology, Weizmann Institute of Science, Rehovot 76100, Israel, and [c]Department of Biology, Technion, Haifa 32000, Israel. *Correspondence e-mail: danc@tx.technion.ac.il, noam@cc.technion.ac.il

Received 24 February 2015
Accepted 26 March 2015

Edited by T. O. Yeates, University of California, USA

Keywords: COPI; coatomer; MHD.

PDB reference: MHD of the COPI δ subunit, 4o8q

Supporting information: this article has supporting information at journals.iucr.org/d

The heptameric COPI coat (coatomer) plays an essential role in vesicular transport in the early secretory system of eukaryotic cells. While the structures of some of the subunits have been determined, that of the δ-COP subunit has not been reported to date. The δ-COP subunit is part of a subcomplex with structural similarity to tetrameric clathrin adaptors (APs), where δ-COP is the structural homologue of the AP μ subunit. Here, the crystal structure of the μ homology domain (MHD) of δ-COP (δ-MHD) obtained by phasing using a combined SAD–MR method is presented at 2.15 Å resolution. The crystallographic asymmetric unit contains two monomers that exhibit short sections of disorder, which may allude to flexible regions of the protein. The δ-MHD is composed of two subdomains connected by unstructured linkers. Comparison between this structure and those of known MHD domains from the APs shows significant differences in the positions of specific loops and β-sheets, as well as a more general change in the relative positions of the protein subdomains. The identified difference may be the major source of cargo-binding specificity. Finally, the crystal structure is used to analyze the potential effect of the I422T mutation in δ-COP previously reported to cause a neurodegenerative phenotype in mice.

1. Introduction

Eukaryotic cells contain several types of transport vesicles that control the movement of proteins among compartments of the secretory system. The coat protein I (COPI) system is responsible for retrograde vesicular trafficking of proteins between Golgi cisternae and from the Golgi to the ER (Lee *et al.*, 2004; Béthune *et al.*, 2006). The COPI coat (coatomer) is a soluble 700 kDa protein complex made up of seven subunits, α-COP, β-COP, β'-COP, γ-COP, δ-COP, ε-COP and ζ-COP (Lowe & Kreis, 1998; Waters *et al.*, 1991), which form a stable complex that shuttles between the cytosol and membranes (Lowe & Kreis, 1996). Each of the subunits is well conserved from yeast to mammals (with the exception of ε-COP, which appears to play a structure-stabilizing role). The COPI complex can be chemically dissociated into two subcomplexes (Pavel *et al.*, 1998): the F-subcomplex, which is comprised of the β, γ, δ and ζ subunits, and the B-subcomplex, composed of the α, β' and ε subunits. Based on protein sequence homology, it has been suggested that the coatomer F-subcomplex is structurally similar to the tetrameric clathrin adaptor, while B-COPI was thought to be functionally equivalent to clathrin (Schledzewski *et al.*, 1999; Watson *et al.*, 2004). More recently, these predictions have been confirmed by crystal structures of the cores of several partial complexes of the coatomer (Yu *et al.*, 2012; Hsia & Hoelz, 2010; Lee & Goldberg, 2010). However, structural information is still unavailable for two of

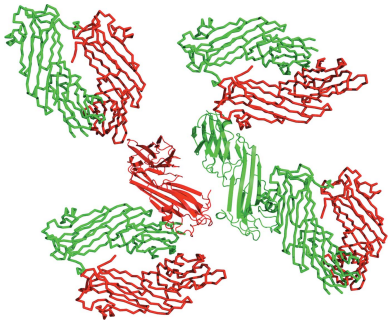

Table 1
Data-collection and final refinement statistics.

Values in parentheses are for the outer shell.

	SeMet†	Native
Data collection		
Space group	$P2_12_12_1$	$P222/P2_12_12_1$‡
Resolution (Å)	39.82–3.02 (3.125–3.011)	50–1.96 (1.99–1.96)
Unit-cell parameters		
a (Å)	42.56	42.1
b (Å)	112.74	110.3
c (Å)	147.72	145.8
$\alpha = \beta = \gamma$ (°)	90.0	90.0
Wavelength (Å)	0.979	0.939
No. of unique reflections	26804 (4183)	43300 (1909)
Multiplicity	4.5	2.8 (2.9)
Data completeness (%)	99.6 (86.6)	88 (77.9)
R_{merge}§ (%)	8.4 (24.9)	5.5 (48.7)
$\langle I/\sigma(I)\rangle$	18.53 (5.43)	28.2 (2.7)
FOM	0.35	
Refinement		
Resolution (Å)		19.89–2.15
No. of reflections		33217
Completeness (%)		87.7
No. of non-H atoms		4053
Protein residues		484
No. of waters		229
R_{cryst}¶ (%)		18.2
R_{free} (%)		22.9
R.m.s.d.		
Bond lengths (Å)		0.008
Angles (°)		1.159
PDB code		4o8q

† The SeMet data set provided the coordinates of a partial model that was used for molecular replacement with the native data set. ‡ The crystallographic data for the native crystal were processed in space group $P222$. The enantiomeric space group $P2_12_12_1$ was determined during the molecular-replacement search. § $R_{merge} = \sum_{hkl}\sum_i |I_i(hkl) - \langle I(hkl)\rangle|/\sum_{hkl}\sum_i I_i(hkl)$, where $I_i(hkl)$ is the intensity of an individual reflection and $\langle I(hkl)\rangle$ is the mean intensity obtained from multiple observations of symmetry-related reflections. ¶ $R_{cryst} = \sum_{hkl}||F_{obs}| - |F_{calc}||/\sum_{hkl}|F_{obs}|$. A randomly omitted 5% of the reflections were used for calculation of R_{free}.

the F-subcomplex subunits: β-COP and δ-COP. The δ-COP subunit shares significant sequence homology with medium (μ) chains of clathrin-associated adaptor complexes (Cosson *et al.*, 1996, 1998). Both proteins contain conserved N-terminal domains followed by more variable C-terminal domains which have been denoted as AP μ-subunit homology domains or μ homology domains (MHDs). Cargo sorting into COPI vesicles is based on the recognition of sorting signals that are found in the cytoplasmic domain of membrane proteins by different coatomer subunits. The MHD of δ-COP (hereafter referred to as δ-MHD) interacts with membrane proteins by recognition of arginine-based sorting signals (R-signals; Michelsen *et al.*, 2007). In monomeric proteins, R-signals act as ER retrieval signals; however, upon the assembly of multi-subunit complexes R-signals can become hidden or rendered inactive by the recruitment of multivalent proteins, thereby allowing ER export of correctly assembled complexes (Mrowiec & Schwappach, 2006; Michelsen *et al.*, 2006).

The region comprised of amino acids 390–412 in bovine δ-COP contributes to the recognition site for R-signals; this region is highly conserved across eukaryotic species, consistent with the evolutionarily conserved recognition of R-based sorting motifs (Michelsen *et al.*, 2007). A second binding site for R-signals is presented by β-COP (Michelsen *et al.*, 2007). Homology modelling of the adaptor-like F-subcomplex based on the crystal structure of the clathrin adaptor 1 core has suggested that the R-signal binding sites in β-COP and δ-COP are in close proximity to each other (Michelsen *et al.*, 2007). An additional interaction mediated through δ-COP is coatomer binding to a short stretch at the carboxyl end of ArfGAP1 that contains a di-aromatic sequence (Rawet *et al.*, 2010).

Understanding the complete structure of the COPI coat will provide an important framework for understanding its function; however, the lack of structural data for some of the subunits presents a significant obstacle to further analysis of COPI-mediated trafficking events. Here, we present the crystal structure of δ-MHD solved to 2.15 Å resolution using a combined SAD–MR method.

2. Methods and materials

2.1. Expression, purification and crystallization of δ-MHD

Escherichia coli BL21(DE3) pLysS (Novagen) host strain transformed with a vector encoding His_6-tagged bovine δ-MHD (amino acids 267–511; Rawet *et al.*, 2010) was grown in 4 ml LB supplemented with the appropriate antibiotics (100 µg ml^{-1} ampicillin and 34 µg ml^{-1} chloramphenicol) overnight at 37°C. This starter solution was used to inoculate 500 ml LB medium with the same antibiotic concentrations as mentioned above. The medium was shaken at 37°C until the mid-logarithmic growth phase was reached at an OD_{600} of ∼0.8. At this point, 0.25–0.5 m*M* isopropyl β-D-1-thio-galactopyranoside was added and the culture was shaken for a further 3–4 h at 37°C. The cells were harvested by centrifugation (7000 rev min^{-1}, 10 min, 4°C) and frozen at −20°C until protein purification was performed.

Frozen cells were lysed using a French pressure cell in 10 m*M* Tris pH 7.5, 200 m*M* NaCl (buffer *A*) plus protease inhibitors and the protein was purified by nickel-affinity chromatography. The protein was further purified by size-exclusion chromatography on Superdex 200 in buffer *A* containing 5 m*M* dithiothreitol (DTT). The protein was then concentrated to ∼8 mg ml^{-1} by ultrafiltration in a centrifugal filter unit with a membrane NMWL of 10 kDa (Amicon Ultra).

The δ-MHD was screened for potential crystallization conditions using the Index crystallization screen (Hampton Research). We also designed a strong interaction R-based sorting motif synthetic peptide (GL Biochem) containing the sequence KLRRRRI (hereafter referred to as R2; Michelsen *et al.*, 2007) for co-crystallization trials. Diffraction-quality crystals were obtained in five different crystallization conditions. All crystals grew within a week and had a rectangular shape and a length of approximately 0.1 mm in the longest dimension. The presence of full-length δ-MHD in the crystals was confirmed by mass-spectrometric analysis (MS) of solubilized crystals at the Smoler Proteomic Center of the Technion.

2.2. Data collection and processing

Most of the crystals produced data sets. A complete data set was obtained from a crystal obtained by co-crystallization of the δ-MHD protein with the R2 peptide, which was grown in 0.4 *M* NaCl, 0.1 *M* HEPES pH 7.5, 18% polyethylene glycol 3350. X-ray diffraction data were collected on beamline ID14-4 at the ESRF, Grenoble, France, where a crystal maintained at 100 K was exposed to a monochromatic X-ray beam at a wavelength of 0.9394 Å. This crystal, hereafter referred to as the native protein crystal, diffracted to 1.9 Å resolution and a complete data set was collected to 2.15 Å (Table 1). Phasing by MR was attempted (*Phaser*; McCoy *et al.*, 2007) using different models built from the homologous μ2 subunit of AP2 [μ2AP2; PDB entry 2jkr (Kelly *et al.*, 2008) or 1i31 (Boll *et al.*, 2002)]; however, no viable solution was found. Therefore, recombinant δ-MHD was expressed in a Met(−) strain of *E. coli* in the presence of selenomethionine (Mechaly *et al.*, 2000) and the resulting protein was crystallized. We collected a full 3.0 Å resolution SAD data set at the Se anomalous diffraction peak wavelength of 0.9791 Å on ID14-4 at the ESRF (Table 1). This data set was collected from a crystal obtained in 0.2 *M* sodium citrate tribasic dehydrate and 20% polyethylene glycol 3350 without the addition of R2 peptide. We processed the data using *XDS* (Kabsch, 2010). *PHENIX* (Adams *et al.*, 2010) was used to solve the structure; ten independent Se atoms were located corresponding to two protein molecules in the asymmetric unit.

2.3. Structure solution and refinement

PHENIX (Adams *et al.*, 2010) was used for experimental phasing and model building; however, only 60% of the amino acids from both chains were clearly built into the electron density. Each of the two monomers in the asymmetric unit contained different gaps in the structure. After multiple attempts to refine the resulting structure, R_{work} and R_{free} reached values of about 35 and 39%, respectively, but stopped decreasing. Further inspection of the refined structure revealed that one of the two independent molecules in the asymmetric unit (chain *A*) had lower individual isotropic temperature factors and much better defined electron-density maps than the other monomer (chain *B*). After the crystallographic data of the native crystal had been reprocessed with *HKL*-2000 (Otwinowski & Minor, 1997), we used this more complete and better resolved molecule (chain *A*) as a model for a molecular-replacement search (MR) using *PhaserMR* (McCoy *et al.*, 2007) as implemented in *PHENIX* (Adams *et al.*, 2010). One solution with two molecules in the asymmetric unit was then obtained with very high discrimination (TFZ = 7.9, LLG = 1853). Unsurprisingly, comparison of the two solutions obtained by SAD and by MR methods showed that one of the two molecules (referred to above as chain *A*) was placed identically in the asymmetric unit while the second monomer was not. The new solution was submitted to further refinement using *AutoBuild* and simulated annealing in *PHENIX* (Adams *et al.*, 2010) with alternate cycles of manual correction using *Coot* (Emsley *et al.*, 2010) and minimization using *phenix.refine* (Adams *et al.*, 2010; Afonine *et al.*, 2012). The structure was refined to final *R* and R_{free} values of 18.2 and 22.8%, respectively (Table 1). The structure of δ-MHD at 2.15 Å resolution was deposited in the PDB as entry 4o8q.

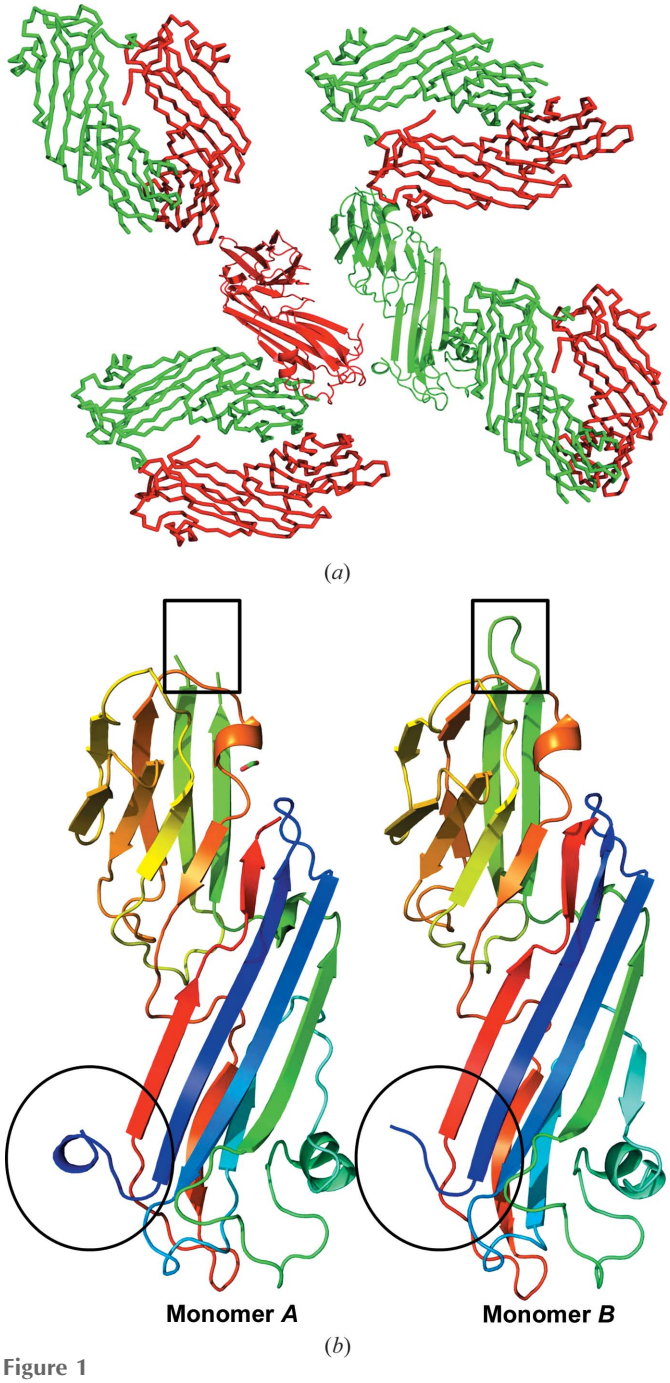

Figure 1
Overall δ-MHD structure. (*a*) Unit-cell interactions. The asymmetric unit is depicted as green (monomer *A*) and red (monomer *B*) cartoons, while symmetry-related molecules are shown in a ribbon display with the same colours. All potential dimers have limited interaction interfaces. (*b*) Comparison between δ-MHD monomers in the asymmetic unit. Monomers are depicted in cartoon representation coloured using the rainbow format implemented by *PyMOL* (DeLano, 2002). The N-terminus (circled) of monomer *A* contains a short helix, while that of monomer *B* is unstructured. The loop containing residues 384–388 (boxed) is absent in monomer *A* but is present in monomer *B*. This loop is neither stabilized nor destabilized by crystal lattice contacts.

3. Results and discussion

3.1. Crystal packing

δ-MHD was found to crystallize in space group $P2_12_12_1$, with unit-cell parameters a = 42.09, b = 110.3, c = 145.79 Å, $\alpha = \beta = \gamma = 90^\circ$. In this space group, the asymmetric unit contains two monomers of δ-MHD (Fig. 1*a*). δ-MHD was characterized by size-exclusion chromatography as forming an aggregation state of two monomers, and we could identify potential dimers in the crystallographic unit cell (Fig. 1*a*). There is no evidence that δ-MHD can be found as a dimer *in vivo*, and *PDBePISA* (Krissinel & Henrick, 2007) could not identify specific interactions that could result in the formation of stable quaternary structures. This is reasonable as each subunit appears only once in the COPI complex, according to the model suggested by Yu *et al.* (2012). In δ-MHD, the N-terminal segment of monomer *A* is in close proximity to the C-terminal segment of monomer *B* (Fig. 1*a*). The association between two δ-MHD monomers in solution does indicate that the heterologously expressed protein retains the ability to form protein–protein interactions without leading to uncontrolled aggregation.

3.2. Structure of δ-MHD

Following refinement, structural differences between the two monomers in the asymmetric unit were apparent. Monomer *A* has an extended N-terminus formed by amino acids 267–269 (Figs. 1*b* and 2*a*). A serine replacing the proline at position 267 is the result of the cloning procedure. The more ordered N-terminus of monomer *A* may result from the stabilizing effect of residues 492–495 of monomer *B*, while no residues from monomer *A* approach the N-terminus of monomer *B* (Fig. 1*a*). Electron density was observed for the entire unstructured loop in monomer *B* (residues 384–388; Figs. 1*b* and 2*b*), for which no interpretable electron density could be obtained in monomer *A*. The vicinity of this loop in both monomers is unaffected by crystal-packing interactions. The *B* factors of the loop built into the electron density (Fig. 2*b*) are significantly higher than for most of the protein, indicating that this loop is intrinsically less stable. In monomer *B*, the β-strand encompassing amino acids Ser451–Ser457 also contains a section with high *B* factors. The resulting misalignment of this β-strand with the two adjacent strands causes the loss of the hydrogen-bonding pattern required for proper β-sheet formation.

Each of the two monomers is composed of two subdomains. Subdomain 1 encompasses residues 267–375 and 472–505 and includes the N-terminus and a β-sandwich composed of a well ordered five-stranded β-sheet associated with a two-stranded β-sheet. A short α-helix closes one side of the sandwich. Subdomain 2 includes residues 376–471 and is composed of a second β-sandwich made up of two four-stranded β-sheets. The general outline of the δ-MHD structure is similar to those of previously determined MHD structures (including those from μ2AP2; Kelly *et al.*, 2008; Collins *et al.*, 2002). Alignment of the entire δ-MHD and the μ2AP2 MHD (Jackson *et al.*, 2010) indicates an overall dissimilarity, with a root-mean-square deviation (r.m.s.d.) of 9.2 Å for all homologous C^α atoms. However, visual inspection shows that this is mainly owing to major differences in the positions of the residues that link the two subdomains (unstructured loops 368–376 and 471–481). Structural alignment between subdomains 2 of δ-MHD and μ2AP2 shows significant similarity (r.m.s.d. of 1.4 Å for all homologous C^α atoms). A similar alignment between subdomains 1 (Fig. 3) shows much larger differences (r.m.s.d. of 6.7 Å) in the domain itself, and also a significant shift in the relative position of subdomain 2 by about 20°. These differences in the positioning of the major structural elements are the most likely reason for our failure to obtain a molecular-replacement solution using the previously determined homologues. The differences in structure between δ-MHD and μ2AP2 may also be a major source of specificity in binding the correct target peptides.

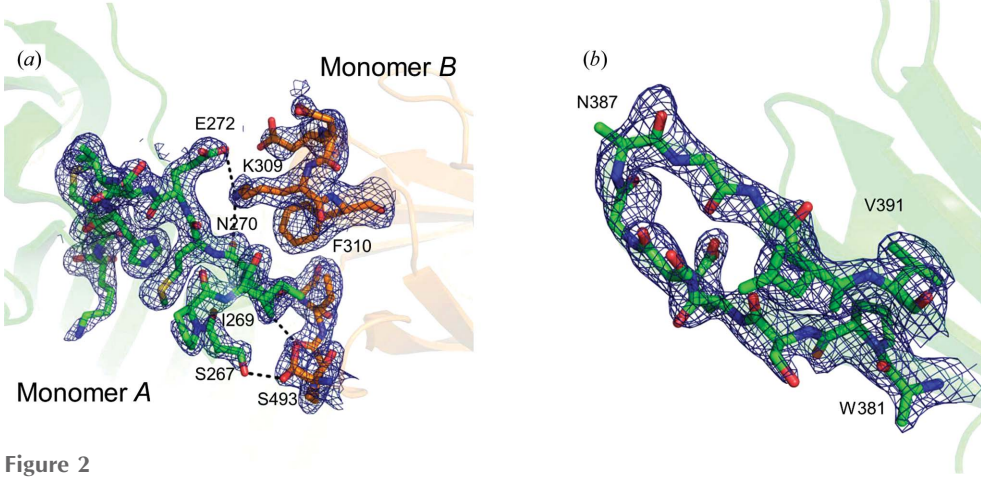

Figure 2
Variable sections of the δ-MHD crystal structures overlaid with a $2F_o - F_c$ electron-density map. The δ-MHD *A* and *B* monomers are shown as green and orange cartoon representations, respectively. The $2F_o - F_c$ electron-density map (blue mesh) is contoured at 1.25σ. (*a*) The interaction interface between the ordered N-terminal residues of monomer *A* (267–277) is stabilized by residues from monomer *B* (residues 309 and 493–494). Residues are depicted in sticks, with N and O atoms coloured blue and red, respectively. (*b*) Overlay of the $2F_o - F_c$ electron-density map onto the ordered 382–390 loop of monomer *B*. No interpretable electron density could be obtained for Asn387, which was modelled as an alanine. There are no crystal-packing interactions that stabilize this loop.

3.3. Functional significance of the δ-MHD structure

The crystal structures of the clathrin adaptor complex have resolved major changes in the position of the μ2AP2 MHD in either the 'closed' (PDB entry 2vgl) or 'open' (PDB entry 2xa7) states (Collins *et al.*, 2002; Jackson *et al.*, 2010). While the N-terminal domain remains relatively constant in its position (with

contacts with the σ and β subunits), the MHD moves almost 40 Å with a significant twisting movement. The surrounding interactions with the σ and α subunits are lost, and the interactions with the β subunit are completely altered. The existence of a 'closed' to 'open' conformational change for the coatomer has not been shown experimentally. However, since the δ-MHD of the coatomer is predicted to play a similar functional role as the μ2AP2 MHD, it is not implausible that a similar movement of the δ-MHD occurs when the coatomer binds cargo. The question that thus arises as a result of this study is whether the crystal structure of the isolated δ-MHD can be attributed to an open or a closed conformation. The two μ2AP2 MHD structures determined when bound in the closed or open forms of AP2 have an overall r.m.s.d. of 1.8 Å for all C^{α} atoms (Fig. 4). Most of the differences are spread out over the entire protein, most likely as a result of the difference in their appropriate binding within the AP2 complex and not owing to a specific conformational change. The β-strands are in nearly the same positions in both subdomains (r.m.s.d.s of 1.7 and 1.3 Å, respectively, using the *SSM* algorithm employed in *Coot*; Emsley *et al.*, 2010); however, owing to large movements in the unstructured strands, the subdomains (described above) display significant changes (18.4 and 16.2 Å, respectively, using the *LSQ* algorithm employed in *Coot*). When we now compare the subdomains of the δ-MHD with the subdomains of the two forms of the μ2AP2 MHD, we see that while the β-strands are mostly positioned in a similar fashion, the overall similarities between the subdomains are quite different. Subdomain 1 of δ-MHD is much more similar to the 'closed' version of μ2AP2 MHD than it is to the 'open' state (r.m.s.d.s of 4.0 and 14.2 Å, respectively). Subdomain 2 of δ-MHD is more similar to the 'open' version of μ2AP2 MHD than it is to the 'closed' state (r.m.s.d.s of 7.0 and 12.7 Å, respectively). Analysis of the two AP2 complexes shows that in the closed form subdomain 2 forms the stronger contacts (with the α subunit), while in the open form it is subdomain 1 that forms more extensive contacts (with the β subunit). We can thus propose that in the isolated form both δ-MHD subdomains are more similar to the less constricted subdomain in the AP2 complex. Since in the δ-MHD crystal lattice both subdomains form extensive contacts (with each subdomain being stabilized by symmetry-related subdomains of the same type; Fig. 1*a*), we suggest that it is specific interactions in AP2 (and most likely in the coatomer as well) that cause the changes in structure, and not just general protein–protein interactions. Upon cargo-dependent movement, the μ2AP2 MHD/δ-MHD shifts to the less constrained form, followed by binding-induced structural change to the relevant subdomain upon rebinding. This flexibility may be necessary for the binding/unbinding of R-based signal peptides to δ-MHD. A significant difference between δ-MHD and both forms of μ2AP2 MHD can be seen at the top of subdomain 2 (Fig. 4, black

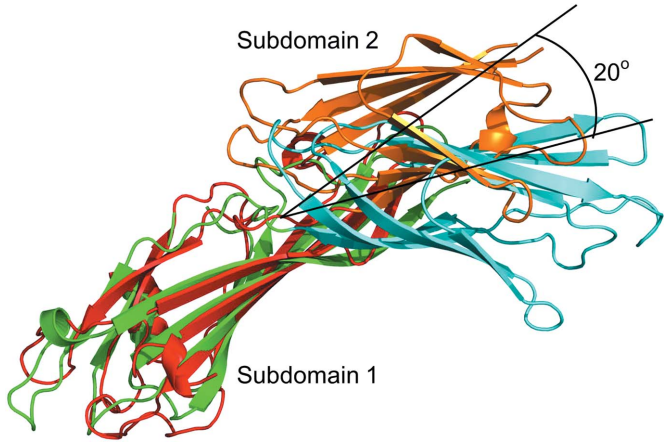

Figure 3
Subdomain orientation changes between δ-MHD and μ2AP2 MHD. Alignment of subdomain 1 of the μ subunit MHD from AP2 (PDB entry 2xa7, green) on subdomain 1 of the δ-MHD monomer *B* (red). Subdomains 2 are coloured cyan and orange, respectively. The r.m.s.d. for all homologous C^{α} atoms of subdomains 1 is 4 Å. Superimposition of subdomains 1 showing that the relative orientations of subdomains 2 are shifted by about 20°.

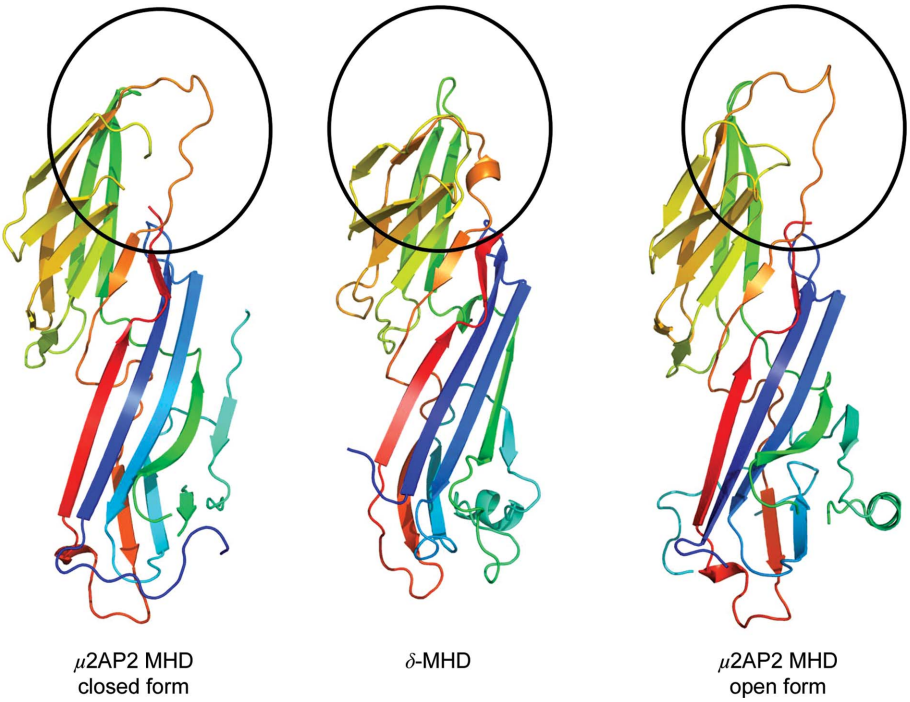

Figure 4
Alignment of δ-MHD and μ2AP2 MHDs. The μ2AP2 MHDs from the closed AP2 complex (PDB entry 2vgl) and the open complex (PDB entry 2xa7) and the coatomer δ-MHD were superimposed on all homologous C^{α} atoms and then shifted without rotation for clearer viewing. The proteins are coloured identically from the N-terminus (blue) to the C-terminus (red). Black circles indicate a variable loop (residues 374–384 according to the 2vgl structure numbering) that becomes compressed and structured in the δ-MHD structure.

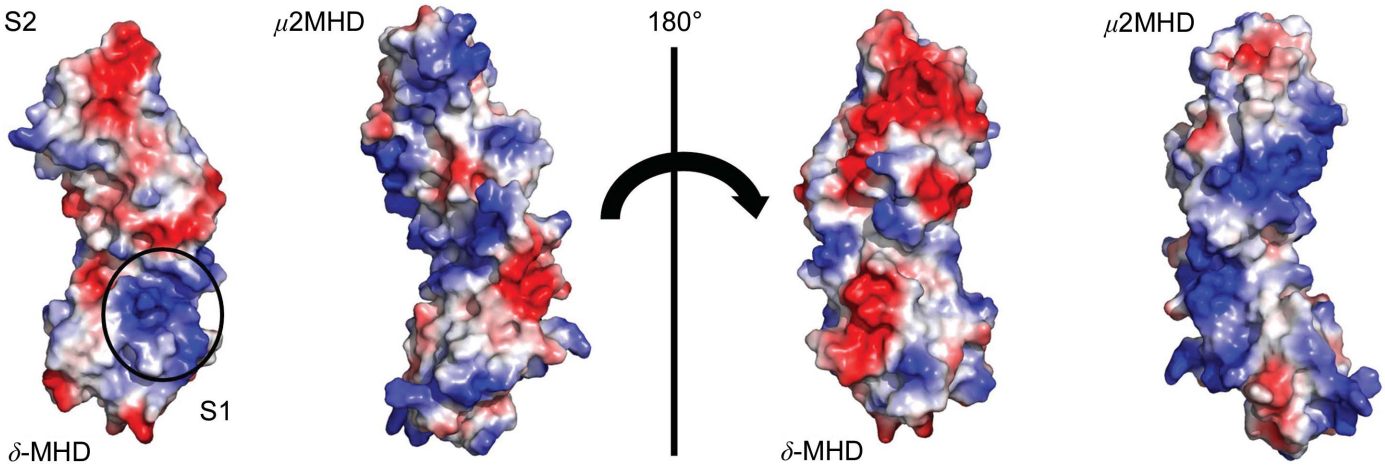

Figure 5
Surface electrostatic potential of the δ-MHD and μ2AP2 MHDs. Surface electrostatic potentials were calculated using *PyMOL*, with positive and negatively charged surfaces depicted in blue and red, respectively. S1 and S2 denote subdomains 1 and 2, respectively. Two faces are shown rotated 180° from each other. The black circle indicates a single strongly positive patch in S1 of δ-MHD which potentially interacts with the β subunit of the coatomer.

circles), where an unstructured section of the protein is rather open in μ2AP2 MHD, while in δ-MHD this section is compacted into the main subdomain body and has a short helix. In the closed AP2 form this stretch is made up of residues 374–384 (Collins *et al.*, 2002) and contacts with the α2 subunit are formed. In the open AP2 form, the same stretch (residues 384–394 in the structure with PDB code 2xa7) makes contacts with the β2 subunit. The changes in position and structure in this section of δ-MHD would appear to indicate that this movement is critical for binding at one of the two positions, and that upon release the section compacts (preventing rebinding) and then reopens upon rebinding in the new site.

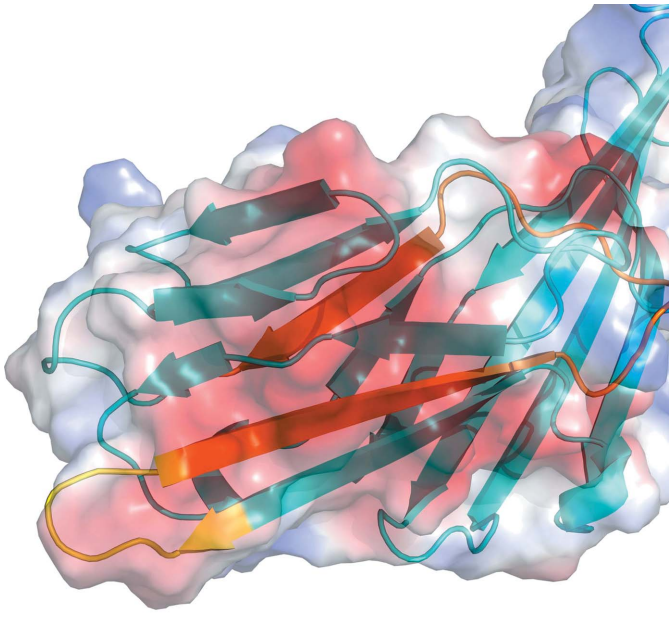

Figure 6
The proposed R-based signal binding site visualized in the δ-MHD structure (monomer *B*). The putative R-based signal binding site (residues 390–412) is shown in orange. These strands are connected to the flexible loop (residues 382–389, in yellow). The surface of the subdomain shows the electrostatic potential calculated using *PyMOL* (DeLano, 2002). The surface above the R-based binding signal site shows significant negative potential.

One of the remarkable differences between δ-MHD and μ2AP2 MHD is in the relative electrostatic potential of the surfaces (Fig. 5). While μ2AP2 MHD is mostly positive, with only small negative patches, δ-MHD has a very negatively charged surface potential on almost its entire surface. Only a single isolated patch on the surface of δ-MHD is significantly positive, which may assist in the proper alignment of the domain in one of the two positions. Using the δ-MHD structure, we were also able to visualize the structure of the putative R-based signal binding site (Fig. 6; residues 390–412). The β-strands that make up the site are connected to the flexible loop (residues 382–389) discussed above. It is possible that cargo binding is assisted by the flexible characteristics of this loop, locking the cargo in place after the initial binding occurs *via* the static β-strand elements.

3.4. Prediction of the effect of the I422T mutation in δ-MHD leading to a neurodegenerative phenotype in mice

Like most coatomer subunits, δ-COP is an essential gene (Faulstich *et al.*, 1996; Xu *et al.*, 2010; Hamamichi *et al.*, 2008). A human disease associated with a δ-COP mutation has not been reported; however, a mouse strain with a δ-COP mutation was found to exhibit coat-colour dilution and ataxic movements (Xu *et al.*, 2010). The mutation, which causes a change from Ile to Thr at position 422 (Supplementary Fig. S1), results in only partial loss of the COPI function. In cells from these mice, the efficiency of protein trafficking through the ER and Golgi may be affected. The mutation does not cause RNA instability or improper processing of the protein, as the expression and localization of ARCN1 are not altered in the nur17 melanocytes, suggesting that the mutation results in a localized effect, possibly affecting an important binding

site. We used *SWISS-MODEL*, optimal docking areas (ODAs), *DUET* and *ERIS* (Arnold *et al.*, 2006; Kiefer *et al.*, 2009; Guex *et al.*, 2009; Fernandez-Recio *et al.*, 2005; Pires *et al.*, 2014; Yin *et al.*, 2007*a*,*b*) to predict the possible effect of this mutation on the δ-MHD structure. The I422T mutation does not appear to disrupt the β-sheet at this position. The mutation site is near a suspected polar protein-interaction surface, adjacent to the suspected R-based signal binding site. The *DUET* and *ERIS* computational servers predict that the I422T missense mutation may destabilize the antiparallel β-sheet. One aspect that is apparent from visual inspection of the δ-MHD structure is that Ile422 is situated opposite Tyr429. Modelling of the Thr422 mutation shows that the hydroxyl is at a hydrogen-bonding distance from the hydroxyl of Tyr429. This additional bond would actually stabilize the positions of the two parallel β-sheets. Thus, the loss in hydrophobic stabilization energy may be compensated in part by hydrogen-bond stabilization (Wilcock *et al.*, 1998), which is compatible with only a partial loss of COPI function.

Acknowledgements

This study was supported by Grant No. 31/11 from the Israel Science Foundation and an award from the Skillman Foundation to DC. We thank the ESRF and the staff of ID14-4 for their assistance in data collection.

References

Adams, P. D. *et al.* (2010). *Acta Cryst.* D**66**, 213–221.
Afonine, P. V., Grosse-Kunstleve, R. W., Echols, N., Headd, J. J., Moriarty, N. W., Mustyakimov, M., Terwilliger, T. C., Urzhumtsev, A., Zwart, P. H. & Adams, P. D. (2012). *Acta Cryst.* D**68**, 352–367.
Arnold, K., Bordoli, L., Kopp, J. & Schwede, T. (2006). *Bioinformatics*, **22**, 195–201.
Béthune, J., Wieland, F. & Moelleken, J. (2006). *J. Membr. Biol.* **211**, 65–79.
Boll, W., Rapoport, I., Brunner, C., Modis, Y., Prehn, S. & Kirchhausen, T. (2002). *Traffic*, **3**, 590–600.
Collins, B. M., McCoy, A. J., Kent, H. M., Evans, P. R. & Owen, D. J. (2002). *Cell*, **109**, 523–535.
Cosson, P., Démollière, C., Hennecke, S., Duden, R. & Letourneur, F. (1996). *EMBO J.* **15**, 1792–1798.
Cosson, P., Lefkir, Y., Démollière, C. & Letourneur, F. (1998). *EMBO J.* **17**, 6863–6870.
DeLano, W. L. (2002). *PyMOL*. http://www.pymol.org.
Emsley, P., Lohkamp, B., Scott, W. G. & Cowtan, K. (2010). *Acta Cryst.* D**66**, 486–501.
Faulstich, D., Auerbach, S., Orci, L., Ravazzola, M., Wegchingel, S., Lottspeich, F., Stenbeck, G., Harter, C., Wieland, F. T. & Tschochner, H. (1996). *J. Cell Biol.* **135**, 53–61.
Fernandez-Recio, J., Totrov, M., Skorodumov, C. & Abagyan, R. (2005). *Proteins*, **58**, 134–143.
Guex, N., Peitsch, M. C. & Schwede, T. (2009). *Electrophoresis*, **30**, S162–S173.
Hamamichi, S., Rivas, R. N., Knight, A. L., Cao, S., Caldwell, K. A. & Caldwell, G. A. (2008). *Proc. Natl Acad. Sci. USA*, **105**, 728–733.
Hsia, K.-C. & Hoelz, A. (2010). *Proc. Natl Acad. Sci. USA*, **107**, 11271–11276.
Jackson, L. P., Kelly, B. T., McCoy, A. J., Gaffry, T., James, L. C., Collins, B. M., Höning, S., Evans, P. R. & Owen, D. J. (2010). *Cell*, **141**, 1220–1229.
Kabsch, W. (2010). *Acta Cryst.* D**66**, 125–132.
Kelly, B. T., McCoy, A. J., Späte, K., Miller, S. E., Evans, P. R., Höning, S. & Owen, D. J. (2008). *Nature (London)*, **456**, 976–979.
Kiefer, F., Arnold, K., Künzli, M., Bordoli, L. & Schwede, T. (2009). *Nucleic Acids Res.* **37**, D387–D392.
Krissinel, E. & Henrick, K. (2007). *J. Mol. Biol.* **372**, 774–797.
Lee, C. & Goldberg, J. (2010). *Cell*, **142**, 123–132.
Lee, M. C., Miller, E. A., Goldberg, J., Orci, L. & Schekman, R. (2004). *Annu. Rev. Cell Dev. Biol.* **20**, 87–123.
Lowe, M. & Kreis, T. E. (1996). *J. Biol. Chem.* **271**, 30725–30730.
Lowe, M. & Kreis, T. E. (1998). *Biochim. Biophys. Acta*, **1404**, 53–66.
McCoy, A. J., Grosse-Kunstleve, R. W., Adams, P. D., Winn, M. D., Storoni, L. C. & Read, R. J. (2007). *J. Appl. Cryst.* **40**, 658–674.
Mechaly, A., Teplitsky, A., Belakhov, V., Baasov, T., Shoham, G. & Shoham, Y. (2000). *J. Biotechnol.* **78**, 83–86.
Michelsen, K., Mrowiec, T., Duderstadt, K. E., Frey, S., Minor, D. L., Mayer, M. P. & Schwappach, B. (2006). *Traffic*, **7**, 903–916.
Michelsen, K., Schmid, V., Metz, J., Heusser, K., Liebel, U., Schwede, T., Spang, A. & Schwappach, B. (2007). *J. Cell Biol.* **179**, 209–217.
Mrowiec, T. & Schwappach, B. (2006). *Biol. Chem.* **387**, 1227–1236.
Otwinowski, Z. & Minor, W. (1997). *Methods Enzymol.* **276**, 307–326.
Pavel, J., Harter, C. & Wieland, F. T. (1998). *Proc. Natl Acad. Sci. USA*, **95**, 2140–2145.
Pires, D. E., Ascher, D. B. & Blundell, T. L. (2014). *Nucleic Acids Res.* **42**, W314–W319.
Rawet, M., Levi-Tal, S., Szafer-Glusman, E., Parnis, A. & Cassel, D. (2010). *Biochem. Biophys. Res. Commun.* **394**, 553–557.
Schledzewski, K., Brinkmann, H. & Mendel, R. R. (1999). *J. Mol. Evol.* **48**, 770–778.
Waters, M. G., Serafini, T. & Rothman, J. E. (1991). *Nature (London)*, **349**, 248–251.
Watson, P. J., Frigerio, G., Collins, B. M., Duden, R. & Owen, D. J. (2004). *Traffic*, **5**, 79–88.
Wilcock, D., Pisabarro, M. T., López-Hernandez, E., Serrano, L. & Coll, M. (1998). *Acta Cryst.* D**54**, 378–385.
Xu, X., Kedlaya, R., Higuchi, H., Ikeda, S., Justice, M. J., Setaluri, V. & Ikeda, A. (2010). *PLoS Genet.* **6**, e1000956.
Yin, S., Ding, F. & Dokholyan, N. V. (2007*a*). *Nature Methods*, **4**, 466–467.
Yin, S., Ding, F. & Dokholyan, N. V. (2007*b*). *Structure*, **15**, 1567–1576.
Yu, X., Breitman, M. & Goldberg, J. (2012). *Cell*, **148**, 530–542.